L³ F-TOUCH: A Wireless GelSight with Decoupled Tactile and Three-axis Force Sensing

Wanlin Li, Meng Wang, Jiarui Li, Yao Su, Devesh K. Jha, Xinyuan Qian,
Kaspar Althoefer and Hangxin Liu

Abstract—GelSight sensors that estimate contact geometry and force by reconstructing the deformation of their soft elastomer from images would yield poor force measurements when the elastomer deforms uniformly or reaches deformation saturation. Here we present an L³ F-TOUCH sensor that considerably enhances the three-axis force sensing capability of typical GelSight sensors. Specifically, the L³ F-TOUCH sensor comprises: (i) an elastomer structure resembling the classic GelSight sensor design for fine-grained contact geometry sensing; and (ii) a mechanically simple suspension structure to enable three-dimensional elastic displacement of the elastomer structure upon contact. Such displacement is tracked by detecting the displacement of an ARTag and is transformed to three-axis contact force via calibration. We further revamp the sensor's optical system by fixing the ARTag on the base and reflecting it to the same camera viewing the elastomer through a mirror. As a result, the tactile and force sensing modes can operate independently, but the entire L³ F-TOUCH remains <u>L</u>ight-weight and <u>L</u>ow-cost while facilitating a wire<u>L</u>ess deployment. Evaluations and experiment results demonstrate that the proposed L³ F-TOUCH sensor compromises GelSight's limitation in force sensing and is more practical compared with equipping commercial three-axis force sensors. Thus, the L³ F-TOUCH could further empower existing Vision-based Tactile Sensors (VBTSs) in replication and deployment. The design is open-sourced at: https://github.com/wangmeng13thu/L3-F-TOUCH.

Index Terms—GelSight sensor, vision-based tactile sensor

I. INTRODUCTION

ACHIEVING human-level dexterity during manipulation and grasping has been a long-standing goal in robotics.

Wanlin Li, Meng Wang, Jiarui Li, Yao Su, and Hangxin Liu are with National Key Laboratory of General Artificial Intelligence, Beijing Institute for General Artificial Intelligence (BIGAI), Beijing 100080, China (e-mail: liwanlin@bigai.ai; wangmeng@bigai.ai; lijiarui@bigai.ai; suyao@bigai.ai; liuhx@bigai.ai).

Jiarui Li is also with Department of Advanced Manufacturing and Robotics, College of Engineering, Peking University, Beijing 100871, China

Devesh K. Jha is with Mitsubishi Electric Research Labs (MERL), Cambridge, MA 02139, USA (e-mail: jha@merl.com).

Xinyuan Qian is with Department of Computer and Communication Engineering, University of Science and Technology Beijing, Beijing, 100083, China (e-mail: qianxy@ustb.edu.cn).

Kaspar Althoefer is with Centre for Advanced Robotics @ Queen Mary (ARQ), Queen Mary University of London, UK (e-mail: k.althoefer@qmul.ac.uk).
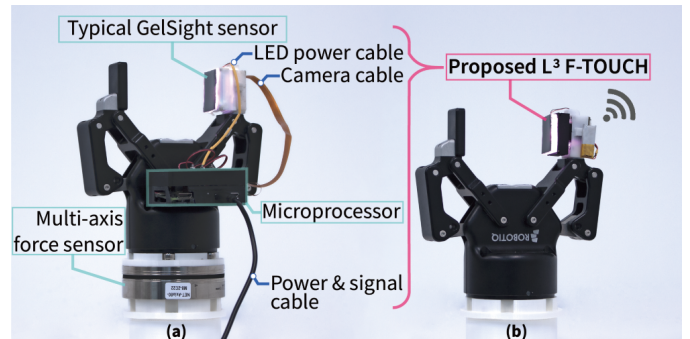
Fig. 1: **Tactile and force sensing in robot manipulation.** (a) A typical integration of a GelSight sensor for fine-grained tactile sensing and a multi-axis force sensor mounted on the manipulator's wrist for force sensing, with complex cabling issues and undesired bulkiness. (b) The proposed L³ F-TOUCH supports concurrent tactile and three-axis force sensing, becoming much easier to deploy.

To accomplish this goal, having a reliable sense of tactile and force is essential for robots. In recent years, Vision-based Tactile Sensor (VBTS), *e.g.* GelSight sensor [1] and its variants [2–7], have emerged as an effective approach to measure tactile and force information. The foundation of GelSight sensing technique involves reconstructing the deformation of a soft elastomer caused by external objects using images captured with an embedded camera. Moreover, normal and shear forces can be inferred from the deformation, in addition to the contact geometry. Due to the advantages of being low-cost, easy-to-replicate, and achieving pixel-level spatial resolution in measurements, GelSight sensors have significantly expanded robots' capabilities in grasping applications, such as handling fragile object [8], manipulating deformable items [9], and classifying materials [10].

However, the force sensing mechanism of GelSight sensors has two limitations: (i) it cannot measure forces when the elastomer deforms uniformly, *i.e.* when touching a large flat surface, because the reconstruction of elastomer's surface normal is hindered as the brightness changes cannot be effectively captured by the camera; (ii) the range of its force sensing is limited by the thickness of its elastomer—it saturates when the elastomer cannot deform further—especially when the latest GelSight designs are becoming slimmer with thin elastomer [3, 4, 11]. Consequently, a multi-axis force sensor, *e.g.* an ATI sensor [12], is typically mounted on the wrist of a robot's arm to complement the GelSight sensor installed at gripper's fingertip when the robot is tasked to perform more forceful grasping and manipulation [4, 13, 14]; a typical

setup is shown in Fig. 1a. This setup is not ideal as it increases the payload of the robot arm, introduces errors when synchronizing and calibrating the two sensors, and measures force far from the actual contact point.

In this paper, we present L^3 F-TOUCH, see Fig. 1b, a novel tactile and force sensor that integrates a mechanically simple suspension structure comprised of stiff parallel springs and an elastomer structure equipped with the GelSight sensing technique. Upon external contact, the elastomer structure not only reconstructs the contact geometry but also experiences three-dimensional elastic displacement that can be transformed to a three-axis force with a significantly larger range compared with that of a GelSight sensor. We further design an optical-based tracking mechanism that tracks the distortion of a marker printed on the fixed suspension base through a mirror, which serves as a simple yet effective indicator of the displacement of the elastomer structure. This mirror reflection design keeps the sensor's form factor small because (i) the same camera viewing the elastomer's deformation is used to track the marker and no new sensory transducer is introduced, and (ii) the overall dimension can be shrunk by tuning the angle of reflection, leading to better compactness.

The design principle behind L^3 F-TOUCH also introduces three advantageous features, *i.e.* the L^3 features, that facilitate deployment of VBTS and future research into this field. Rather than the usage of multi-axis force sensors, L^3 F-TOUCH is **Light-weight** and **Low-cost** as the suspension structure and the tracking mechanism do not require new sensors or complex structures, resulting in minimal increases in manufacturing costs, size, or weight compared to GelSight sensors. Furthermore, the concurrent but decoupled tactile and force measurement derived from one image permit us to customize a **wireLess** camera module for real-time image streaming. Although the use of WiFi for remote image acquisition was presented in [15], we incorporate a power supply circuit to allow the entire sensor to run on a portable battery, further reducing the sensor's form factor and cabling complexity in deployment.

The contributions of proposed L^3 F-TOUCH are two-folded. Principally, we design a new vision-based three-axis force sensing mechanism that can be seamlessly integrated into existing VBTS without interference with tactile sensing. Practically, we make the components of L^3 F-TOUCH publicly available to empower existing VBTSs in replication and deployment.

A. Related Work

Various tactile and force sensors have been developed with different sensing principles, such as multi-axis force sensors (*e.g.* transducers and strain gauges [12]), high-end tactile sensors (*e.g.* BioTac [16]), e-skins [17, 18] and low-cost tactile sensors made from force sensitive resistor or piezoresistive material [19]. However, they are usually at high cost [12, 16], difficult for reproduction and deployment [17, 18] or with limited point-force sensing capability [19].

To overcome these limitations, VBTS (*e.g.* GelSight [1]), as a low-cost solution, is proposed. They can not only estimate

contact normal force from Gel's deformation, but also infer shear forces *indirectly* from the movements of printed marker arrays [20, 21] or ultraviolet (UV) marker arrays [22–24]. Furthermore, following variants of VBTS focus on minimizing sensor dimension for easier deployment, which include using mirror reflection to reposition camera (*e.g.* Gelslim [3], GelSight wedge [4], GelSight Fin Ray [25]), introducing a delicate silicone layer (*e.g.* DIGIT [11], DenseTact [5, 26], DTact [6], DelTact [27]), or incorporating tactile fingertip sensors [28, 29]. While the elastomer of these sensors become thinner for compactness, their force sensing range is sacrificed, resulting in easier saturation.

Other than integrating a separated and high-cost force/torque sensor, several attempts [2, 30, 31] are made to improve VBTS's force sensing capability. Notably, an F-TOUCH sensor that equipped a spring-suspension structure under the Gel was developed to integrate three-axis force sensing capability to fine-grained tactile sensing [2]. However, the suspension structure in [2] has two shortcomings: (i) its displacement is computed from three distorted dots printed underneath the Gel, which requires inpainting on the acquired tactile imprint before processing, damaging the tactile information; (ii) the camera viewing the Gel is fixed to the base and would zoom in and out during contact due to the suspension's displacement, degrading its reliability. In this work, the presented L^3 F-TOUCH first eliminates such interference by reflecting a marker to the camera's view through a mirror, without overlapping with tactile imprints. Then, the camera is also suspended together with the elastomer structure, so that its views remain stationary. The new design introduced by L^3 F-TOUCH also allows us to further reduce the sensor's form factor; see Tab. I for comparison with F-TOUCH.

B. Overview

The remainder of this paper is organized as follows. Sec. II presents the hardware design and fabrication details of our L^3 F-TOUCH sensor. Sec. III and Sec. IV describes the procedures for force calibration and sensor evaluation. The capabilities and advantages of L^3 F-TOUCH are further demonstrated through a series of experiments in Sec. V. Finally, we conclude the paper with a discussion in Sec. VI.

II. SENSOR DESIGN AND FABRICATION

The proposed L^3 F-TOUCH sensor aims to enhance the GelSight sensor's force sensing while inheriting its advantages of being (i) compact and lightweight for installation on the jaw gripper's fingertips, and (ii) cost-effective, easy-to-replicate, and easy-to-deploy. To achieve these goals, L^3 F-TOUCH sensor adopts the classic GelSight technique to fabricate an elastomer structure for sensing contact geometry and introduces a spring suspension structure to enable the elastomer's floating motions under contact. These motions are tracked by a marker-based visual detection scheme and transformed into a three-axis contact force. Thus, L^3 F-TOUCH sensor can be made in a small form factor and applied to a wide range of applications. Below we first briefly describe the major components of L^3 F-TOUCH, followed by its detailed fabrication process.
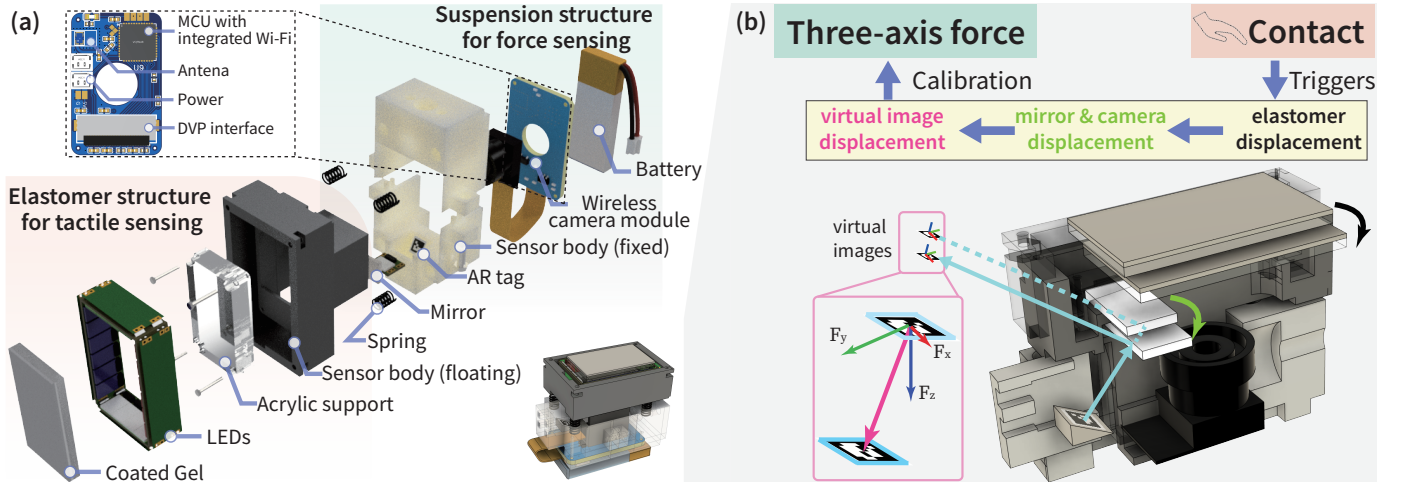
Fig. 2: **L³ F-TOUCH sensor design and its force sensing principle.** (a) The sensor consists of two parts: The elastomer structure attains a super high spatial resolution in sensing contact geometry. Using stiff springs, the suspension structure allows the elastomer to displace upon contact. A PCB is designed to remotely transmit camera images to a workstation and to power the sensor with a battery. (b) Under contact, the ARTag fixed in the suspension would be projected to a different image coordinate in the camera's view due to the displacement of the mirror installed underneath the elastomer. Such displacements are transformed to three-axis contact forces through calibration.

A. Elastomer Structure

Following the design principle of GelSight sensor, the elastomer structure of L³ F-TOUCH consists of five major components, as shown in the left part of Fig. 2a. The elastomer is made from transparent gel, with a marker array and opaque matte reflective coating printed on top. A clear acrylic board is placed under the elastomer for support, and an internal multi-color LED light source is attached around it to provide uniform illumination. The sensor body encloses the above components while holding a mirror and a micro camera with a wide-angle lens inside. Of note, although the sensor body is suspended to enable floating motions when contact occurs, the camera view to the Gel remains stationary during motion.

B. Suspension Structure

To extend the force sensing capability, a mechanically simple but reliable suspension structure comprised of stiff parallel springs is proposed. As shown in the right part of Fig. 2a, the fixed sensor body includes a "$4 \times 4\_50$" ArUco tag with a size of $3\ mm$ affixed to a $40°$ tilted slope, a PCB to acquire camera images and transmit them wirelessly to the workstation, and a portable battery that powers the entire sensor. Four parallel springs are installed in the fixed sensor body to support the floating elastomer structure. The tilted angle and the size of the ARTag are empirically found to promote observability.

With this suspension structure, the contact force exerted on the sensor not only deforms the Gel but also causes multi-axis floating motions of the elastomer structure due to the elastic compression of the parallel springs. The camera inside the elastomer structure observes both the tactile imprint with a constant boundary for reconstructing contact geometry and the ARTag's projected pose, which differs as the mirror moves, for measuring contact force. Importantly, the tactile imprint and the tag's pose are decoupled, simplifying the sensor's calibration process.

C. Fabrication Details

Wireless Camera Module: We manufactured a PCB (see Fig. 2a) to make the sensor more compact and easier to deploy. It integrates a power supply circuit for all electronic components, a Digital Video Port (DVP) connecting to the camera, and an ESP32 MCU with a 2.4G ceramic antenna for streaming the captured images to a remote workstation. An RTSP server runs in the MCU to stream images in M-JPEG format with a resolution of 640×480 at a frame rate of 26 FPS. Sec. IV provides a further study on the balance between sampling frequency, latency, and image resolution. As a result, the dimension of the L³ F-TOUCH is minimized (see Tab. I), and the entire sensor runs on a $3.7V$ LiPo battery.

Illumination: We used surface-mounted LEDs in four colors (red, green, blue, and white) to illuminate the coated Gel and a white LED to light up the ARTag. To optimize the image quality captured by the camera, we chose LUXEON 2835 Color Line SMD LED which is not only small in size ($3.5 \times 2.8 \times 0.7\ mm$) but also provides a full-color palette for a wide spectrum range. The spectrum response of both the camera and the LEDs were compared for the RGB color selection. Additionally, gray filers (VViViD Air-Tint Dark Air-Release Vinyl Wrap Film) and diffusers (3M Diffuser 3635-70) were stuck to the side of the acrylic sheet to effectively improve the contrast and uniformity of tactile frames [4].

Coated Gel: As the suspension structure enables large-range force measurement, it is possible to reduce the thickness and hardness of the coated Gel. We used Smooth-On Solaris part A&B (Shore A 15) as the clear base with a thickness of $1.5\ mm$. Smooth-On Slacker was then added as the silicone thinner with the weighted ratio of $1:1:3$ (part A: part B: thinner). For the coating layer, we used mill-resistant matte oil to protect the silicone rubber's surface and mixed it with spherical aluminum powder to produce a Lambertian surface. We airbrushed the diluted mixture onto the base's surface to form a reflective and protective coating layer. Note that we
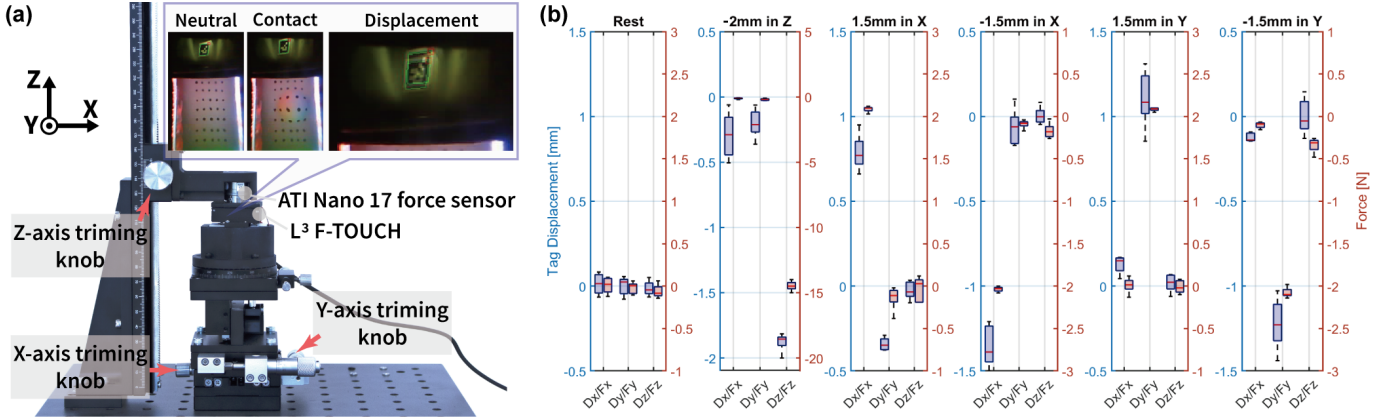
Fig. 3: **The force calibration setup**. (a) Under contact, the camera views the Gel deformation and the reflected ARTag's displacement in the same frame, enabling concurrent, but independent tactile and force sensing. (b) By trimming the sensor in 5 directions, the distributions of the three-axis force and the three-axis displacement of the virtual ARTag are acquired.

TABLE I: **Comparison of four tactile and force sensing setups:** (i) Nano17 [12] + GelSight [32], (ii) Nano17 + DIGIT [11], (iii) F-TOUCH [2], and (iv) the proposed L^3 F-TOUCH . L^3 F-TOUCH demonstrates strong comprehensive advantages in terms of size, weight, cost, communications and force measurements.

Sensors	Nano17	GelSight	DIGIT	F-TOUCH	L^3 **F-TOUCH**
Size [mm]	17×17×15	50×80×40	20×27×18	50×80×40	25×40×35
Weight [g]	12	NA	20	~ 70	25
Cost [$]	5000+	~ 30	15	40	31
Comm.	Wired	Wired	Wired	Wired	Wireless
RES	Point Touch	640×480	640×480	640×480	640×480
Force Meas.	Global	Local	None	Global	Global

printed a 5×7 black marker array with Smooth-On Silc Pig black colorant on the top surface to replicate the established force sensing mechanism of the original GelSight technique, which was not needed for L^3 F-TOUCH and was only for comparison; see Sec. III-B for details.

D. Summary

Tab. I summarizes the key parameters in terms of size, weight, cost, communications, and force measurements of L^3 F-TOUCH compared with alternative setups that can acquire tactile information and three-axis force. For instance, a Gel-Sight or a DIGIT needs to be combined with a Nano17 to acquire the aforementioned data. Apart from the increased space occupation and weight, such costs and communications will be very heavy. Therefore, L^3 F-TOUCH is more economical and more convenient to use. Although GelSight-like sensors can be made using off-the-shelf materials with a cost of just

TABLE II: The bill of materials (BOM) of L^3 F-TOUCH sensor.

|	Part	Description	Qty	Cost
Elastomer	Camera	OV2640 with 160° lens	1	$3
	LEDs	RGBWhite SMD LEDs	20	$5
	Mirror	$5 \times 10 \times 1 \ mm$	1	$1
	Gel	Base + marker + coating	1	$5
	3D printed housing	Elastomer structure body	1	$3
Suspension	Spring	$0.4 \times 3 \times 5 \ mm$	4	$1
	Electronic components	PCB, MCU, etc.	1	$6
	Battary	400mAh 1-cell LiPo	1	$2
	3D printed housing	Suspension structure body	2	$3
	Misc items	Glue, printed Aruco marker	2	$2
			Total costs	**$31**
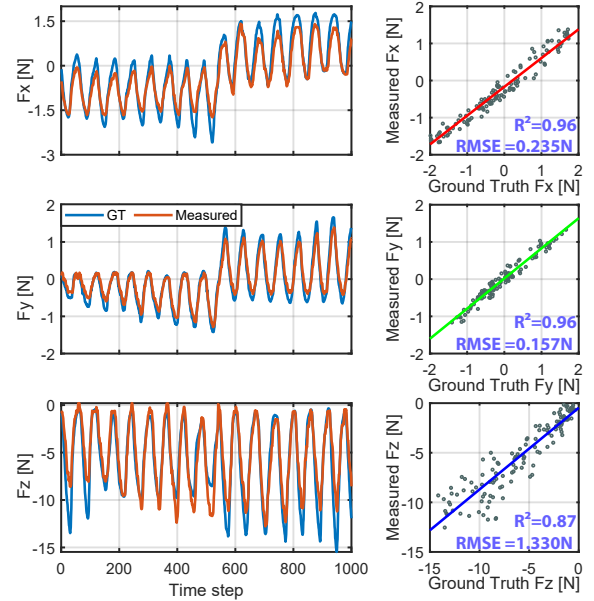
Fig. 4: **Force calibration results.** *Left:* The force measurements obtained from our L^3 F-TOUCH sensor demonstrate a strong correlation with those from the ATI Nano 17. *Right:* The L^3 F-TOUCH sensor achieves high accuracy and linearity in both the x and y axes, as evidenced by low RMSE and high R^2. Although the results in z axis are not as ideal, considering its larger range, they remain satisfactory.

tens of dollars, their commercial versions could cost hundreds. As a result, we open-source the entire hardware design and processing software of the L^3 F-TOUCH to further promote its potential applications. Tab. II provides the bill of materials of the L^3 F-TOUCH and the cost for each major component.

III. SENSOR CALIBRATION

This section describes the calibration of the L^3 F-TOUCH sensor from two aspects: multi-axis force calibration and tactile imprint calibration. Since these two modalities are decoupled, each calibration process can be operated independently. Besides, due to the distortion from the wide-lens camera, we first apply a standard camera calibration to rectify the captured frame [33].

A. Force Calibration

In our design, the external force $\mathbf{F} = [F_x, F_y, F_z]^T$ applied to the sensor results in the displacement of the mirrored tag $\mathbf{D} = [D_x, D_y, D_z]^T$ in the camera's image coordinates; see Fig. 2b. Thus, force calibration establishes the appropriate transformation between $\mathbf{F}$ and $\mathbf{D}$ in a simplified linear form:

$$\mathbf{K}_{3\times3} \cdot \mathbf{D} + \text{Bias} = \mathbf{F}, \tag{1}$$

where $\mathbf{K}_{3\times3}$ maps the coupled effects between the displacement and the force. Given the camera's calibration parameters and the ARTag's geometric dimensions, the mirrored tag's displacement $\mathbf{D}$ can be efficiently measured.

The calibration setup is shown in Fig. 3a. We used an XYZ 3-Axis linear stage trimming platform to control the displacement of the floating elastomer structure, and the corresponding force reading that serves as the ground-truth is measured by an ATI Nano17 6-axis F/T sensor. The ATI sensor is placed on the Z stage and trimmed down to initiate contact with the elastomer structure. This state is referred to as the *Rest* condition, (*i.e.* 0 *mm* in z). Then, we collected a dataset of tag displacements under five controlled conditions: trimming ±1.5 *mm* in the x-axis, ±1.5 *mm* in the y-axis, and -2 *mm* in the z-axis. In each condition, the trim positions not in the axis-of-interest are set to 0. The correlations between the resulting displacement of the mirrored ARTag $\mathbf{D}$ and the corresponding forces $\mathbf{F}$ are shown in Fig. 3b. Based on this dataset, we solve for Eq. (1) by the least squares method, and Fig. 4 shows the calibrated result.

B. Tactile Mode Calibration

The elastomer structure of the L³ F-TOUCH functions as a GelSight sensor. To leverage its advantage of sensing contact geometry, a tactile calibration is performed by following the established procedure for GelSight. Below we briefly describe the procedure and refer interested readers to [1] for details. It is also possible to calibrate GelSight using inverse FEM based on elastostatic theory [3], which is more challenging to conduct and could be less accurate due to the Gel's nonlinear deformation.

Reconstructing contact geometry: The GelSight technique measures deformation upon contact by mapping the RGB color intensity of the frame to corresponding horizontal and vertical surface gradients g_x, g_y and integrating them at each pixel to obtain the depth. To build the look-up table that maps RGB to g_x, g_y [32], we collected tactile frames with a known-size metallic sphere pressing upon the Gel. In each frame, the sphere casts a circular contact whose center c_x, c_y and radius r are measured to calculate the gradient g_x, g_y based on the contact volume of the sphere; the gradients correspond to pixel intensity within the contact region.

Measuring contact force: Based on the reconstructed contact geometry, distributed normal force can be estimated from the depth deformation at each marker printed on the Gel. Utilizing the displacement of the marker array, contact shear force can be inferred as well [4]; however, such displacement only positively correlates to the shear force rather than an actual measurement, which is considered a
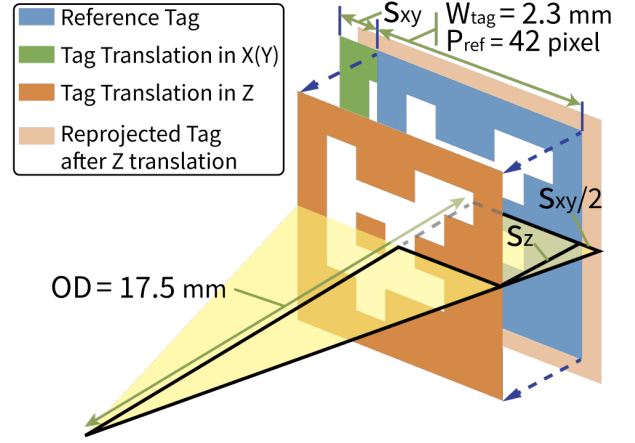

Fig. 5: **Schematic view of the tag translation and sensitivity.** The optical model is simplified as a symmetric diagram around the optical axis. The green tag indicates an X(Y) translation s_{xy} which results in a 1 pixel translation of the tag image. The red tag indicates a Z translation s_z which results in 1 pixel width change of the tag image.

limitation of GelSight technique in force sensing. Notably, L³ F-TOUCH alleviates this limitation by using the suspension structure to measure force. We apply the force calibration to the elastomer structure solely for comparative studies that demonstrate L³ F-TOUCH 's advantages in force sensing.

IV. SENSOR EVALUATION

We characterize the force sensing capability of L³ F-TOUCH sensor, *i.e.* the efficacy of the suspension structure, from the following six aspects. Due to the intensive study conducted on GelSight sensors in the literature [1], we do not provide a further evaluation of the elastomer structure.

Linearity: Based on the calibration data from Fig. 3 and the regression model obtained from Eq. (1), the right part of Fig. 4 shows the linearity result of L³ F-TOUCH sensor, where the root mean square error ($RMSE$) values are 0.2346 N, 0.1573 N, and 1.33 N, while the R-square values are $0.96, 0.96$ and 0.87 in F_x, F_y and F_z. The fitting in z axis is less ideal than that in xy plane due to the sensor sensitivity investigated below.

Range: The maximum output is determined by the reliability of the transformation between the displacement of the mirrored tag and the force. From the calibration results observed in Fig. 4, the range is determined as ±2 N in the xy plane and 12 N in the z direction. Within this range, the sensor maintains high linearity.

Sensitivity: Based on the optical model of L³ F-TOUCH conceptualized in Fig. 5, we compute the minimal detectable change of the ARTag and correspond that to the output force according to the calibration matrix. Knowing the default discernible resolution of the tag is $R = 1$ $pixel$ [34], the tag's actual width to the camera $W_{tag} = 3.0$ $mm \times \cos 40° = 2.3$ mm as it is printed with a $40°$ inclination, and the tag occupies $P_{ref} = 42$ $pixel$ in the image plane under the rest condition, we can calculate the minimum detectable displacement of the tag in x and y direction from the image:

$$s_{xy} = \frac{W_{tag}}{P_{ref}} R = \frac{2.3}{42} \times 1 = 0.055 \ mm/pixel. \tag{2}$$
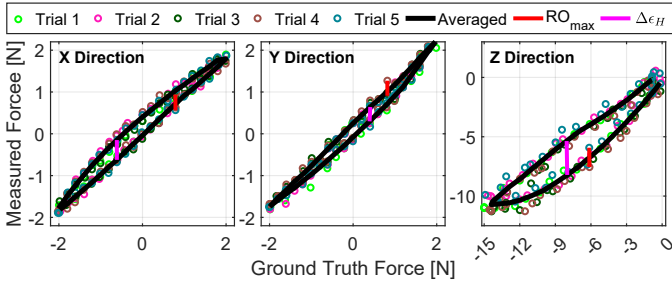
Fig. 6: **Repeatability and hysteresis properties of the L^3 F-TOUCH sensor.** Five trials of identical loading and unloading processes for all three directions were conducted and shown by the circles. They were averaged and plotted as the black curve with smoothing to better reflect the sensor's hysteresis.

TABLE III: **Frame rate and latency comparison between L^3 F-TOUCH and wired GelSight sensor.** Under six different display resolutions, each sensor would run for three 5-min trials. The frame rate was computed based on the number of images received in the workstation within the time interval. The latency would fluctuate over time and was manually monitored; only a range was provided.

Resolution	GelSight		L^3 F-TOUCH	
	frame rate [FPS]	latency [ms]	frame rate [FPS]	latency [ms]
QQVGA(160 × 120)	30		28	
HQVGA(240×176)	30		27	
QVGA(320×240)	30	100 ∼ 150	27	300 ∼ 350
HVGA(480×320)	30		26	
VGA(640×480)	30		26	
SVGA(800×600)	30		20	

Similarly, given the object distance $OD = 17.5\ mm$, the tag's minimal detectable displacement in z direction is

$$s_z = \frac{OD}{(W_{tag} + s_{xy})/2} \frac{s_{xy}}{2} = 0.409\ mm/pixel. \quad (3)$$

Given the calibration matrix $K_{3\times3}$, we obtain the corresponding sensitivity of three-axis forces S_x, S_y, and S_z as follows:

$$\begin{bmatrix} S_x \\ S_y \\ S_z \end{bmatrix} = \begin{bmatrix} & K_{3\times3} & \end{bmatrix} \cdot \begin{bmatrix} s_{xy} \\ s_{xy} \\ s_z \end{bmatrix} = \begin{bmatrix} 0.070 \\ 0.067 \\ 0.324 \end{bmatrix} N/pixel. \quad (4)$$

As the sensitivity in x and y direction is about 5 times finer than that in z, the force measurement in z direction would have a larger variation.

Repeatability: Using the calibration setting in Fig. 3a, we control the x, y, z-axis trimming knob to repeat the loading and unloading process across 5 trials. The comparison between measured and ground truth forces are plotted as the dashed lines in Fig. 6. Taking the Z-axis as an example due to its central role in grasping, the repeatability of L^3 F-TOUCH is calculated as:

$$Repeatability(z) = \frac{\Delta RO_{max}}{\varepsilon_{SO}} \times 100\% = 11\%, \quad (5)$$

where $\varepsilon_{SO} = 12\ N$ is the maximal F_z applied in this study and $\Delta RO_{max} = 1.63\ N$ is the maximal difference at the same timestep across all trials. Following the same procedure, the repeatability of F_x and F_y is calculated as 10% and 9%, respectively.

Hysteresis: The solid black curve in Fig. 6 is the average of the 5 trials measured above with a moving average smoothing. Based on this curve, the maximum difference in normal direction between two processes $\Delta \epsilon_H$ is observed as $2.86\ N$, and the hysteresis is calculated as

$$Hysteresis(z) = \frac{\Delta \epsilon_H}{\varepsilon_{SO}} \times 100\% = 25\%. \quad (6)$$

Considering that the output values during loading are larger than those during unloading, the main reason could be attributed to the viscoelasticity effect in the connection of compression springs during sensor manufacturing. Similarly, the hysteresis in the shear direction of F_x and F_y is 13% and 9%, respectively.

Bandwidth and latency: We tested 6 most commonly used display resolutions listed in Tab. III for image acquisition and streaming, and compared them with a wired version of GelSight sensor with the same hardware specification. While the traditional GelSight sensor maintains a stable 30 FPS across all settings, the proposed L^3 F-TOUCH has a 26 FPS for VGA (640×480) which balances the information preservation and the frame rate. On the other hand, sensor latency is not significantly affected by resolutions. But wireless communication introduced a higher latency in streaming due to network conditions, transferring protocol, and decoding configurations, which can be further optimized to a level comparable to that of wired GelSight [35]. Overall, the wireless feature of L^3 F-TOUCH does not degrade the sensor's data acquisition compared with that of classic GelSight sensor [1], but it enables a much easier setup under different scenarios.

V. EXPERIMENT AND APPLICATION

This section presents three unique advantages of the proposed L^3 F-TOUCH sensor. First, we demonstrated its force sensing range is significantly enlarged by the suspension structure. Second, we validated the necessity of integrating both tactile and force sensing in L^3 F-TOUCH when grasping fragile objects or large objects with a flat surface.
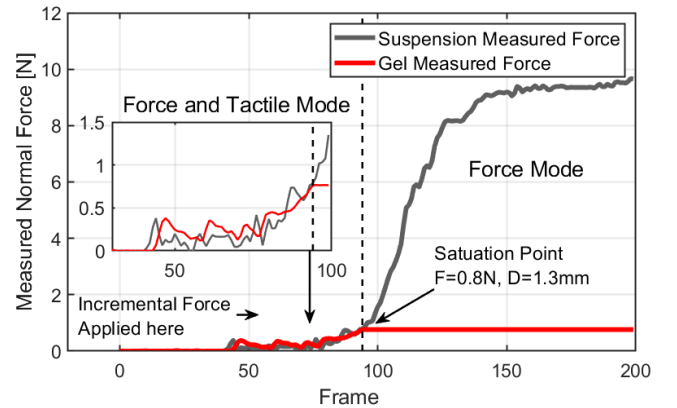

Fig. 7: **The force measurement obtained from the suspension structure and the elastomer of the L^3 F-TOUCH .** The force sensing of the elastomer was saturated at $0.8\ N$ with the maximal deformation of $1.3\ mm$. Incorporating the suspension underneath the elastomer resulted in a 10 times larger force sensing range.
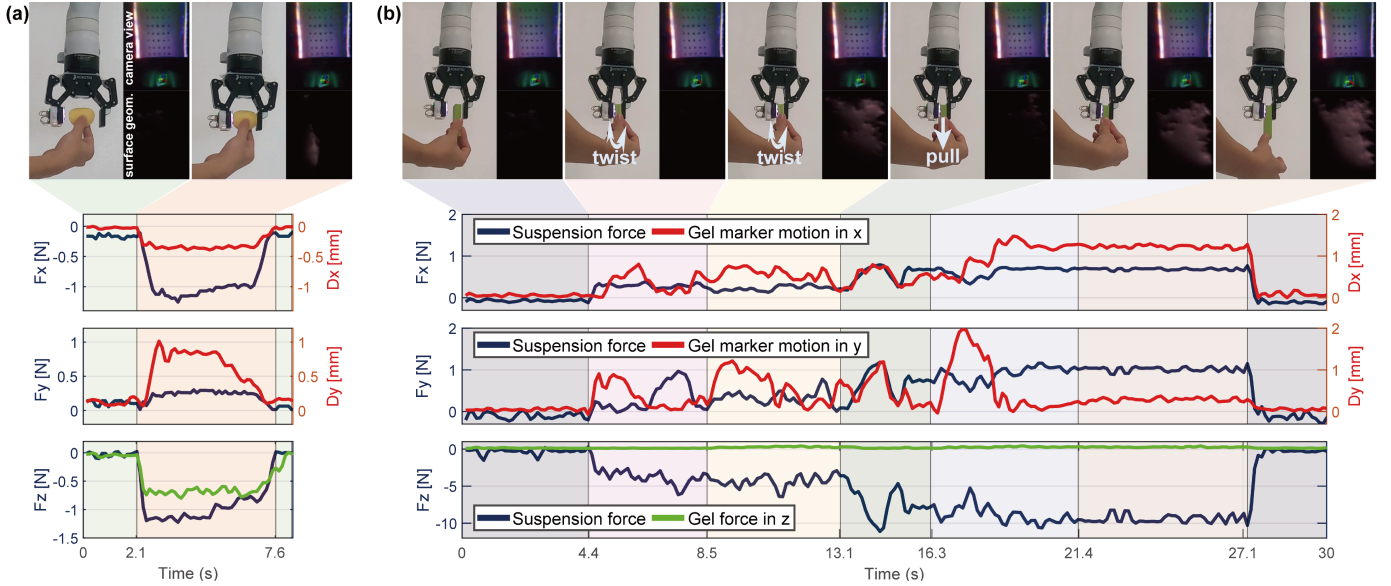
Fig. 8: **L^3 F-TOUCH sensor's contact geometry and force sensing capability.** (a) Gripping a piece of fragile potato chip. (b) Gripping a flat brick with smooth contact. The L^3 F-TOUCH produced reliable three-axis force measurement in both cases whereas the elastomer alone became insufficient. The elastomer augmented three-axis forces with contact geometry, producing richer tactile data.

A. Extended Force Sensing

In this task, we used the trimming platform in Fig. 3 to press a $4\ mm$ diameter sphere against the sensor in the vertical direction and compared the force measurements obtained from the L^3 F-TOUCH and the elastomer structure alone. The results are illustrated in Fig. 7. As can be seen that the force derived from the Gel's deformation was quickly saturated at $0.8\ N$ when it reached a $1.3\ mm$ deformation which was close to the thickness of the Gel ($1.5\ mm$). In contrast, the suspension structure achieved a range of $10\ N$ reliably, effectively overcoming the limitation of force sensing using elastomer alone or using GelSight sensors in general.

Although making the coated Gel thicker seems like a straightforward solution to extend traditional GelSight sensors' force sensing range (*e.g.* HySenSe [36]), it would cause several complications, such as increased sensor size, shear deformation, poor illumination condition, blurry images taken from the camera, and other challenges that necessitate significant engineering efforts to address in practice.

B. Usability in Grasping

To confirm L^3 F-TOUCH's tactile and force sensing capabilities in object grasping, we installed the sensor at a Robotiq 2F-85 gripper mounted to a Kinova Gen3 manipulator and conducted two grasping tasks: gripping a piece of potato chip and holding a flat brick.

Fragile object grasping: Here the robot was tasked with gripping a piece of potato chip without crashing it, see Fig. 8a. The gripper started to close at $2.1s$ and held its position when the Gel of elastomer deformed beyond $0.5\ mm$ until the gripper reopened at $7.6s$. We could see that the elastomer, which measures force by Gel deformation, and the suspension structure, which measures force by elastic displacement, produced similar force readings in the normal direction

(F_z). This indicates that the proposed suspension structure is as effective as typical GelSight sensors in capturing small forces. In addition, the suspension structure provides direct measurements of the force in xy plane, whereas GelSight only provides that indirectly (*i.e.* by mark motions). The elastomer structure and the suspension structure of the L^3 F-TOUCH together create a synergy between contact geometry and reliable three-axis force measurement, resulting in richer tactile information in robot grasping.

Large flat-surface object grasping: A number of daily objects feature smooth and flat surfaces that facilitate comfortable human grasping. But GelSight and akin sensors struggle to measure contact forces when gripping these objects, as the Gel deforms uniformly upon contact, lacking sufficient surface gradient variations. Fig. 8b shows the sensor readings and some snapshots of the robot grasping a toy brick. The surface geometry reconstructed from Gel deformation provides limited information, except when the human forcefully twisted the brick. Thus, the normal force reading from the elastomer remained flat. The L^3 F-TOUCH sensor effectively overcame this limitation. It reliably measured the three-axis force throughout the process and sensitively detected slip and increased gripping force when the human tried to pull away the brick. These outcomes demonstrate the efficacy of the proposed L^3 F-TOUCH sensor.

VI. CONCLUSION

This paper presented L^3 F-TOUCH sensor that enhanced the force sensing capabilities of classic GelSight sensors while achieving a <u>L</u>ight-weight, <u>L</u>ow-cost and wire<u>L</u>ess design. The sensor's elastomer structure, similar to that of a GelSight sensor, can measure contact geometry with a super high spatial resolution. Meanwhile, the compact suspension structure allows the elastomer to displace upon contact, which projects an ARTag printed on the base differently to the camera view

through a mirror. A calibration method was subsequently developed to transform the tag's movements to three-axis force; thus, L^3 F-TOUCH achieved a more reliable and much larger range of force measurements than a GelSight does. The L^3 F-TOUCH further integrated a wireless camera module to reduce its size and deployment effort, opening up new opportunities for using VBTS.

Future work will focus on extending the sensor's capabilities from three-axis force to six-axis force and torque while remaining accurate and compact. Enhancing the sensor's sensitivity can be achieved by adjusting the suspension structure, and the wireless transmission feature can be further improved by optimizing protocol and decoding configurations. These advancements can enable the sense of touch for more dynamic and agile robots in manipulation tasks, even in aerial manipulation settings [37].

REFERENCES

[1] W. Yuan, S. Dong, and E. H. Adelson, "Gelsight: High-resolution robot tactile sensors for estimating geometry and force," *Sensors*, vol. 17, no. 12, p. 2762, 2017.
[2] W. Li, A. Alomainy, I. Vitanov, Y. Noh, P. Qi, and K. Althoefer, "F-touch sensor: Concurrent geometry perception and multi-axis force measurement," *IEEE Sensors Journal*, vol. 21, no. 4, pp. 4300–4309, 2020.
[3] D. Ma, E. Donlon, S. Dong, and A. Rodriguez, "Dense tactile force estimation using gelslim and inverse fem," in *IEEE International Conference on Robotics and Automation (ICRA)*, 2019.
[4] S. Wang, Y. She, B. Romero, and E. Adelson, "Gelsight wedge: Measuring high-resolution 3d contact geometry with a compact robot finger," in *IEEE International Conference on Robotics and Automation (ICRA)*, 2021.
[5] W. K. Do and M. Kennedy, "Densetact: Optical tactile sensor for dense shape reconstruction," in *IEEE International Conference on Robotics and Automation (ICRA)*, 2022.
[6] C. Lin, Z. Lin, S. Wang, and H. Xu, "Dtact: A vision-based tactile sensor that measures high-resolution 3d geometry directly from darkness," *arXiv preprint arXiv:2209.13916*, 2022.
[7] K. Althoefer, Y. Ling, W. Li, X. Qian, W. W. Lee, and P. Qi, "A miniaturised camera-based multi-modal tactile sensor," in *IEEE International Conference on Robotics and Automation (ICRA)*, 2023.
[8] W. Yuan, R. Li, M. A. Srinivasan, and E. H. Adelson, "Measurement of shear and slip with a gelsight tactile sensor," in *IEEE International Conference on Robotics and Automation (ICRA)*, 2015.
[9] Y. She, S. Wang, S. Dong, N. Sunil, A. Rodriguez, and E. Adelson, "Cable manipulation with a tactile-reactive gripper," *International Journal of Robotics Research (IJRR)*, vol. 40, no. 12-14, pp. 1385–1401, 2021.
[10] W. Yuan, Y. Mo, S. Wang, and E. H. Adelson, "Active clothing material perception using tactile sensing and deep learning," in *IEEE International Conference on Robotics and Automation (ICRA)*, 2018.
[11] M. Lambeta, P.-W. Chou, S. Tian, B. Yang, B. Maloon, V. R. Most, D. Stroud, R. Santos, A. Byagowi, G. Kammerer, *et al.*, "Digit: A novel design for a low-cost compact high-resolution tactile sensor with application to in-hand manipulation," *IEEE Robotics and Automation Letters (RA-L)*, vol. 5, no. 3, pp. 3838–3845, 2020.
[12] "Ati multi-axis force/torque sensors family." https://www.ati-ia.com/products/ft/sensors.aspx.
[13] H. Liu, C. Zhang, Y. Zhu, C. Jiang, and S.-C. Zhu, "Mirroring without overimitation: Learning functionally equivalent manipulation actions," in *AAAI Conference on Artificial Intelligence (AAAI)*, 2019.
[14] H. Tugal, K. Cetin, Y. Petillot, M. Dunnigan, and M. S. Erden, "Manipulation at optimum locations for maximum force transmission with mobile robots under environmental disturbances," *Autonomous Robots*, vol. 46, no. 6, pp. 769–782, 2022.
[15] A. C. Abad, D. Reid, and A. Ranasinghe, "Haptitemp: A next-generation thermosensitive gelsight-like visuotactile sensor," *IEEE Sensors Journal*, vol. 22, no. 3, pp. 2722–2734, 2021.
[16] J. A. Fishel and G. E. Loeb, "Sensing tactile microvibrations with the biotac—comparison with human sensitivity," in *International conference on biomedical robotics and biomechatronics (BioRob)*, IEEE, 2012.
[17] J. Park, M. Kim, Y. Lee, H. S. Lee, and H. Ko, "Fingertip skin–inspired microstructured ferroelectric skins discriminate static/dynamic pressure and temperature stimuli," *Science advances*, vol. 1, no. 9, p. e1500661, 2015.
[18] Y. Yu, J. Li, S. A. Solomon, J. Min, J. Tu, W. Guo, C. Xu, Y. Song, and W. Gao, "All-printed soft human-machine interface for robotic physicochemical sensing," *Science Robotics*, vol. 7, no. 67, p. eabn0495, 2022.
[19] H. Liu, X. Xie, M. Millar, M. Edmonds, F. Gao, Y. Zhu, V. J. Santos, B. Rothrock, and S.-C. Zhu, "A glove-based system for studying hand-object manipulation via joint pose and force sensing," in *IEEE/RSJ International Conference on Intelligent Robots and Systems (IROS)*, 2017.
[20] A. Tandon, P. Shukla, and H. K. Patel, "Review of transduction techniques for tactile sensors and a comparative analysis of commercial sensors," in *International Conference on Multidisciplinary Research & Practice*, 2015.
[21] S. Zhang, Z. Chen, Y. Gao, W. Wan, J. Shan, H. Xue, F. Sun, Y. Yang, and B. Fang, "Hardware technology of vision-based tactile sensor: A review," *IEEE Sensors Journal*, 2022.
[22] A. C. Abad and A. Ranasinghe, "Low-cost gelsight with uv markings: Feature extraction of objects using alexnet and optical flow without 3d image reconstruction," in *IEEE International Conference on Robotics and Automation (ICRA)*, IEEE, 2020.
[23] W. Kim, W. D. Kim, J.-J. Kim, C.-H. Kim, and J. Kim, "Uvtac: Switchable uv marker-based tactile sensing finger for effective force estimation and object localization," *IEEE Robotics and Automation Letters (RA-L)*, vol. 7, no. 3, pp. 6036–6043, 2022.
[24] Q. Wang, Y. Du, and M. Y. Wang, "Spectac: A visual-tactile dual-modality sensor using uv illumination," in *IEEE International Conference on Robotics and Automation (ICRA)*, 2022.
[25] S. Q. Liu, Y. Ma, and E. H. Adelson, "Gelsight baby fin ray: A compact, compliant, flexible finger with high-resolution tactile sensing," *arXiv preprint arXiv:2303.14883*, 2023.
[26] W. K. Do, B. Jurewicz, and M. Kennedy III, "Densetact 2.0: Optical tactile sensor for shape and force reconstruction," *arXiv preprint arXiv:2209.10122*, 2022.
[27] G. Zhang, Y. Du, H. Yu, and M. Y. Wang, "Deltact: A vision-based tactile sensor using a dense color pattern," *IEEE Robotics and Automation Letters (RA-L)*, vol. 7, no. 4, pp. 10778–10785, 2022.
[28] B. Romero, F. Veiga, and E. Adelson, "Soft, round, high resolution tactile fingertip sensors for dexterous robotic manipulation," in *IEEE International Conference on Robotics and Automation (ICRA)*, 2020.
[29] S. Q. Liu, L. Z. Yañez, and E. H. Adelson, "Gelsight endoflex: A soft endoskeleton hand with continuous high-resolution tactile sensing," *arXiv preprint arXiv:2303.17935*, 2023.
[30] K. Nozu and K. Shimonomura, "Robotic bolt insertion and tightening based on in-hand object localization and force sensing," in *IEEE/ASME International Conference on Advanced Intelligent Mechatronics (AIM)*, 2018.
[31] R. Ouyang and R. Howe, "Low-cost fiducial-based 6-axis force-torque sensor," in *IEEE International Conference on Robotics and Automation (ICRA)*, 2020.
[32] S. Dong, W. Yuan, and E. H. Adelson, "Improved gelsight tactile sensor for measuring geometry and slip," in *IEEE/RSJ International Conference on Intelligent Robots and Systems (IROS)*, 2017.
[33] J. Kannala and S. S. Brandt, "A generic camera model and calibration method for conventional, wide-angle, and fish-eye lenses," *IEEE Transactions on Pattern Analysis and Machine Intelligence (TPAMI)*, vol. 28, no. 8, pp. 1335–1340, 2006.
[34] "Aruco marker detection." https://docs.opencv.org/4.x/d9/d6a/group__aruco.html.
[35] M. Zorrilla, Á. Martín, F. Mogollón, J. García, and I. G. Olaizola, "End to end solution for interactive on demand 3d media on home network devices," in *International Symposium on Broadband Multimedia Systems and Broadcasting*, IEEE, 2012.
[36] O. C. Kara, N. Ikoma, and F. Alambeigi, "Hysense: A hyper-sensitive and high-fidelity vision-based tactile sensor," in *IEEE Sensors*, 2022.
[37] Y. Su, J. Li, Z. Jiao, M. Wang, C. Chu, H. Li, Y. Zhu, and H. Liu, "Sequential manipulation planning for over-actuated unmanned aerial manipulators," in *IEEE/RSJ International Conference on Intelligent Robots and Systems (IROS)*, 2023.